HHS Public Access

Author manuscript

ACS Nano. Author manuscript; available in PMC 2024 May 23.

Published in final edited form as:

ACS Nano. 2023 May 23; 17(10): 9280–9289. doi:10.1021/acsnano.3c00583.

Multimodal Optothermal Manipulations along Various Surfaces

Hongru Ding[#],
Walker Department of Mechanical Engineering, The University of Texas at Austin, Austin, Texas 78712, United States

Pavana Siddhartha Kollipara[#],
Walker Department of Mechanical Engineering, The University of Texas at Austin, Austin, Texas 78712, United States

Kan Yao[#],
Walker Department of Mechanical Engineering, The University of Texas at Austin, Austin, Texas 78712, United States; Materials Science & Engineering Program and Texas Materials Institute, The University of Texas at Austin, Austin, Texas 78712, United States

Yiran Chang,
Department of Molecular Biosciences, The University of Texas at Austin, Austin, Texas 78712, United States

Daniel J. Dickinson,
Department of Molecular Biosciences, The University of Texas at Austin, Austin, Texas 78712, United States

Yuebing Zheng
Walker Department of Mechanical Engineering, The University of Texas at Austin, Austin, Texas 78712, United States; Materials Science & Engineering Program and Texas Materials Institute, The University of Texas at Austin, Austin, Texas 78712, United States

Abstract

Optical tweezers have provided tremendous opportunities for fundamental studies and applications in the life sciences, chemistry, and physics by offering contact-free manipulation of small objects. However, it requires sophisticated real-time imaging and feedback systems for conventional

Corresponding Author Yuebing Zheng – *Walker Department of Mechanical Engineering, The University of Texas at Austin, Austin, Texas 78712, United States; Materials Science & Engineering Program and Texas Materials Institute, The University of Texas at Austin, Austin, Texas 78712, United States;* zheng@austin.utexas.edu.

Author Contributions

H.D. and Y.Z. conceived the idea for this study. H.D. prepared materials and worked on the experiments. P.K., K.Y., and H.D. conducted the simulations. Y.C. and D.D. prepared *C. elegans* and their embryos. Y.Z. supervised the project. H.D. wrote the manuscript with the input of all other authors.

[#]H.D., P.K., and K.Y. contributed equally to this work.

Supporting Information

The Supporting Information is available free of charge at https://pubs.acs.org/doi/10.1021/acsnano.3c00583.

Simulations of light– matter interactions for optical force analysis and temperature fields, time-resolved optical images showing thermoelectric repelling and trapping of PS microparticles, simulations of net force on PS microparticles, simulations of optothermal forces and their dependence on optical power intensity, measured trapping stiffness of PS microparticles, measured rotation rate of PS microparticles, measured temperature field of a Si microbead heated by a laser beam, simulation of force and torque acting on PS nanoparticles, time-resolved optical images showing the optical injection and *in vivo* manipulation of a Si nanoparticle (PDF)

The authors declare no competing financial interest.

optical tweezers to achieve controlled motion of micro/nanoparticles along textured surfaces, which are required for such applications as high-resolution near-field characterizations of cell membranes with nanoparticles as probes. In addition, most optical tweezers systems are limited to single manipulation modes, restricting their broader applications. Herein, we develop an optothermal platform that enables the multimodal manipulation of micro/nanoparticles along various surfaces. Specifically, we achieve the manipulation of micro/nanoparticles through the synergy between the optical and thermal forces, which arise due to the temperature gradient self-generated by the particles absorbing the light. With a simple control of the laser beam, we achieve five switchable working modes [i.e., tweezing, rotating, rolling (toward), rolling (away), and shooting] for the versatile manipulation of both synthesized particles and biological cells along various substrates. More interestingly, we realize the manipulation of micro/nanoparticles on rough surfaces of live worms and their embryos for localized control of biological functions. By enabling the three-dimensional control of micro/nano-objects along various surfaces, including topologically uneven biological tissues, our multimodal optothermal platform will become a powerful tool in life sciences, nanotechnology, and colloidal sciences.

Graphical Abstract

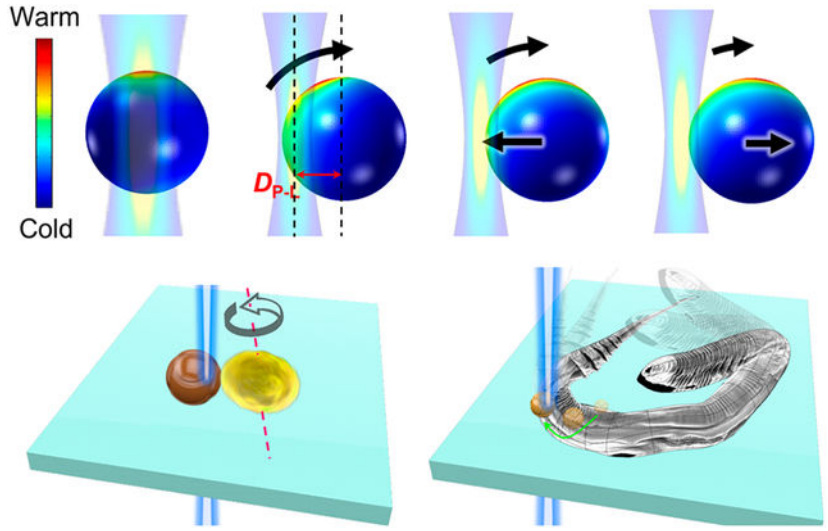

Keywords

optical manipulation; micro/nanoparticles; multimodal manipulation; single-cell manipulation; optical heating

Optical tweezers provide a noncontact method to manipulate micro- and nanoscale entities with light.[1] The tweezers were awarded the Nobel Prize in Physics 2018 for their applications to biological systems.[2,3] However, optical tweezers have a severe limitation of using high optical powers when the refractive index contrast between the object and its surroundings is minimal, which can cause photon damage to many fragile objects, including some biological cells.[4] To overcome this limitation, optothermal manipulation techniques have been proposed as a means of controlling targets regardless of their optical

properties using temperature fields generated by low laser powers.[5] So far, optothermal manipulation platforms have been developed based on thermal forces generated from thermophoresis,[6,7] thermoelectricity,[8,9] thermal convection,[10,11] and thermal depletion,[12,13] leading to dynamic manipulation of diverse micro/nano-objects of varying shapes and sizes. Additionally, different manipulation modes, including tweezing,[8,14] printing,[15,16] pushing,[17-19] pulling,[20,21] and rotation,[22-25] have been achieved independently. Moreover, advanced light steering devices with states controlled by algorithms have been exploited to achieve programmable heat-mediated optical manipulation of particles with high spatiotemporal precision.[26-28]

Despite these advances, there are still two major technical obstacles that hinder the broader biomedical applications of optothermal manipulation, including the realization of multimodal nanorobots in complex *in vivo* environments for nanosurgery. One is that most studies achieved only single-mode manipulation of a colloidal particle in nonbiocompatible solutions, which restricts their direct translation to the manipulation of biological samples. The other is the requirement of substrates with high light-to-heat conversion rates, which limits the optothermal technique to two-dimensional manipulation of target objects along the limited special substrates.[29,28]

Herein, we present a optothermal manipulation technique that overcomes the obstacles by allowing for the multimodal manipulation of micro/nano-objects on various surfaces. The proposed technique can switch between different modes on demand by simply adjusting the particle-laser distance (D_{P-L}) or optical power intensity (I). With the capability of manipulating particles along arbitrarily rough surfaces, including topologically uneven biological tissue surfaces and small living animals, the platform has the potential to be a powerful tool in various fields such as the life sciences, nanorobotics, and colloidal sciences.

RESULTS AND DISCUSSION

General Concept.

The key concept of the multimodal optical manipulation platform is shown in Figure 1. First, a light-absorbing particle is heated and a nonuniform temperature field is generated within the particle and surrounding liquid in a few microseconds. Then, the molecules and ions in the solution diffuse along the temperature gradient, generating several thermal forces on the particle. Last, the thermal forces work in tandem with the optical forces to simultaneously control the translation and rotation motions of the particle. For a proof-of-concept demonstration, a 2.8-μm polystyrene (PS) particle containing 12% iron oxide is selected as the light-absorbing particle and is immersed in a 5 mM NaCl solution with 4.5 wt % polyethylene glycol (PEG) sealed in a glass microchamber. As shown in Figure 1b, a temperature rise of around 18 K can be measured at the particle center upon the illumination of a 532 nm laser beam at the power intensity of 0.23 mW/μm^2 (see Methods for measurement details). A finite element analysis was performed to simulate the light-to-heat conversion within the microparticle, and the generated microscale temperature increase matches well with the experiments (see Methods for simulation details). The simulated temperature field and electric field are illustrated in Figure 1c,d and Supplementary Figure S1, respectively. Temperature gradients can lead to directed movements of molecules and

ions. Depending on solvation entropy, distinct tiny entities display diverse thermodiffusion behaviors.[30] In the localized temperature field, PEG molecules diffuse from the hot region to the cold region, generating a nonuniform osmotic pressure on the particle surface, which pushes the particle toward the hot region.[12,31] This effect is counted by the depletion force (F_D). Similarly, Na^+ and Cl^- ions also show hot-to-cold thermophoretic motions, but with different drift velocities ($\upsilon_{Na}{}^+ > \upsilon_{Cl}{}^-$). The resulting distinct spatial distributions of the two counterions produce a thermoelectric (TE) field that is directed toward the hot spot. When the TE field interacts with negatively charged objects, the effective thermoelectric force (F_{TE}) repels that particle away from the hot spot.[8,32,33] TE fields can also be obtained through the thermophoretic separation of other ion pairs.[34] Therefore, F_{TE} can be modulated on demand by changing the ions in the solution (Supplementary Figure S2). Besides, an optical force (F_O) also plays a critical role in particle translation and rotation.[35,36] Therefore, the PS microsphere can be manipulated over all the degrees of freedom via the synergy of F_D, F_{TE}, and F_O.

The synergy of F_D, F_{TE}, and F_O can be tailored by changing D_{P-L} and I due to the strong dependence of F_D and F_{TE} on the temperature field and the dependence of F_O on the EM field. More specifically, dominated by the thermal diffusion of molecules and ions, the magnitudes of F_D and F_{TE} increase with the magnitude of the temperature gradient, and meanwhile, the directions of the two thermal forces change with the direction of the temperature gradient.[8,12] As shown in Figure 1e, the simulated temperature distribution on the particle surface changes with D_{P-L}, and so do F_D and F_{TE}. Moreover, F_O can be tuned by the EM field which is related to D_{P-L} and the convergence of the laser beam.[1] Optical torque (M_O) generated from the distribution of nonuniform beam intensity and radiation pressure is sensitive to D_{P-L} and the convergence of the laser beam as well.[36] Accordingly, D_{P-L} and I can be used to tailor the forces and torque to achieve the multimodal micro/nanomanipulation as shown in Figure 1e.

The description of all modes of manipulation is as follows. *Tweezing mode*: The particle is trapped and can achieve inplane translation as the incident laser moves. The beam illuminates the center of the particle ($D_{P-L} \approx 0$) and any deviation of the particle from the beam center leads to a restoring force that helps to retain the trapping of the particle. By continuously moving the position of the laser, the object can follow the laser beam and be transported freely on the substrate. Compared to the beam for the rest four modes, a more loosely focused beam is used here to obtain an attractive force trap (see Supplementary Figure S3 for more details). *Rotating mode*: As D_{P-L} increases to an intermediate value, the particle can also achieve out-of-plane rotation without translations. At a specific location, a force balance among F_D, F_{TE}, and F_O can be attained, holding the particle, while M_O powers a steady rotation. *Rolling (toward) mode*: When D_{P-L} is further increased, combined rotation and translation, i.e., rolling, of the object can be achieved. As the temperature distribution and EM field change with D_{P-L} three forces reduce in magnitude. Meanwhile, the directions of F_D, F_{TE}, and F_O change, leading to an increment of the x component of the three forces. Accordingly, the particle experiences a restoring force along the x-axis. The force along with M_O drives the particle to roll toward the incident light beam. *Rolling (away) mode*: When

D_{P-L} is increased to another threshold, the particle can roll away from the beam under a repulsive net force and M_O. At a large distance, all forces are significantly reduced due to a small temperature gradient and a weak EM field. However, F_{TE} decays slower than F_D and F_O,[23] giving rise to a net force pointing away from the beam. Particularly, we have also achieved the fifth mode, shooting mode. When a light-absorbing particle is trapped and heated by the incident light, another particle (transparent or light-absorbing) can be shot away from the heated light-absorbing particle under the long-range repulsive F_{TE}.

Modeling and Force Analysis.

To validate the proposed multimodal platform, we built a multiphysics model in COMSOL, a package based on finite-element method (FEM), to simulate the light–matter interactions and light-to-heat conversion, from which the forces exerted on the PS microparticle in different working modes can be analyzed (see Supplementary Note S1 for modeling details). The depletion force is defined as $F_D = -\oint ck_BT\, dA_r\hat{n}$ (c: local PEG concentration, k_B: Boltzmann constant, T: local temperature, dA_r: differential area element on the particle surface, $\hat{n}$: unit vector normal to the particle surface). The TE force was calculated by integrating the parallel components of the TE field at the rotor surface: $F_{TE} = \oint \sigma_r E_{TE,\parallel} dA_r$ (σ_r: surface charge density of the particle, $E_{TE,\parallel}$: tangential component of the TE field along the particle surface). The optical force and torque were both calculated based on the time-averaged form of the Maxwell stress tensor $\overline{\overline{T}}_M$,[37] defined by surface integrals as $\boldsymbol{F}_O = \oint \overline{\overline{T}}_M \cdot \hat{n} dA$ and $\boldsymbol{M}_O = \oint (\vec{r} \times \overline{\overline{T}}_M) \cdot \hat{\boldsymbol{n}} dA$, respectively, with $\vec{r}$ the radius vector. In principle, the optical force can be further decomposed into a scattering force and a gradient force. However, the separation scheme requires substantially more complicated treatment.[38] We therefore attributed the optical force components along the z- and x-axis as the scattering force and gradient force, respectively, based on their well-established origins under the ray optics approximation.[39]

In order to quantitatively expound each working mode, we decoupled the translational and rotational motions of the target particle. The x component of the total force ($F_x = F_{TE,x} + F_{D,x} + F_{O,x}$) determines the translational behavior of the particle and the y component of optical torque ($M_{O,y}$) regulates the rotation behavior. As shown in Figure 2a, $F_{D,x}$ and $F_{O,x}$ are negative, dragging the PS microsphere back toward the laser beam. In comparison, $F_{TE,x}$ pushes the particle away. Since the magnitude of $F_{TE,x}$ is greater than its counterparts, F_x keeps positive until D_{P-L} is increased to 1.25 μm, where a force balance is reached. This is close to the experimental observation (~1.1 μm). At this D_{P-L}, the rotating mode is established: F_x is around zero trapping the particle, while a large $M_{O,y}$ of 302.8 pN·μm/(W/μm^2) powers the fast rotation of the particle (Figure 2b). At D_{P-L} between 1.25 and 2.00 μm, the negative F_x will always guide the motor back to the position where force balance is reached. This is the rolling (toward) mode. Interestingly, the rolling (away) mode is realized at a D_{P-L} ranging from 2.00 to 3.00 μm, where a small positive F_x (1–10 fN) nudges the particle away and meanwhile a small $M_{O,y}$ of 5–50 pN·μm/(W/μm^2) drives the rotation, resulting in the rolling (away) mode. It is worth noting that $F_{TE,x}$, $F_{D,x}$, $F_{O,x}$, and $M_{O,y}$ all increase with the optical power intensity (Supplementary Figure S4). Therefore, an

effective rolling (away) mode can be realized by simply increasing optical power intensity for larger F_x and $M_{O,y}$ shadowing Brownian motion. To achieve the tweezing mode, we reduced the convergence of light by tuning the numerical aperture (NA) from 1.3 to 0.5 for lower heating efficiency and a stronger optical gradient force. As shown in Supplementary Figure S3, a trap well can be achieved at I as low as 0.028 mW/μm^2. It is noted that the trapping force stems from the depletion force and optical gradient force, and the latter is dominating. As a control experiment, the light-absorbing PS microparticle was observed repelled in a 5 mM NaCl solution without PEG molecules (Supplementary Movie S1), validating the role of depletion force in the tweezing mode.

The effect of thermal convection on manipulation is not included in the current model because a thin chamber (thickness: ~120 μm) was used to suppress thermal convection in this system. Based on the previous work,[26] the estimated thermal convective drag force on a 2.8-μm PS particle working at different modes in all experiments is 1 order of magnitude smaller than the other three forces (F_x, $F_{D,x}$, $F_{TE,x}$). Note that thermal convection and Marangoni flow[40] may be considered under intense laser illumination. In addition, the thermo-osmosis flow from the substrate is neglected due to the highly charged substrate and the thick chamber.[41-43] The thermophoretic motion induced by the thermo-osmotic salt-ion flow around particles is also trivial compared to the thermoelectric effect in electrolyte solutions with large Seebeck coefficients, such as the NaCl solution herein.[44-46]

Multimodal Manipulation of Micro/Nanoparticles.

As a demonstration, 2.8-μm PS microparticles containing iron dioxide were dispersed in a NaCl/PEG solution to experimentally verify our physical model and exhibit the on-demand versatile multimodal manipulation of single particles. As shown in Figure 3a and Supplementary Movie S2, a PS microsphere was trapped using a laser beam ($I = 0.064\,\text{mW}\,/\,\mu\text{m}^2$; $D_{P-L} = 0\ \mu$m) and dynamically transported along prescribed paths at a velocity of ~3.8 μm/s. To assess the trapping stability of the tweezing mode, we measured the trapping stiffness by processing the trajectories of a trapped 2.8-μm PS particle (Supplementary Figure S5). The rotating mode was achieved as D_{P-L} was set as ~1.1 μm and I was increased to 0.23 mW/μm^2 (Figure 3b and Supplementary Movie S3). To quantitatively characterize the out-of-plane rotation, we labeled the PS microparticles with fluorescent nanobeads through streptavidin–biotin binding. A rotation rate of 60 rpm was observed for the PS microsphere as shown in the successive fluorescent images. In the rotating mode, trapping stiffness was measured as 5.6 pN/μm (Supplementary Figure S6). Note that an out-of-plane rotation is realized herein, which has been proven extremely challenging for other optical manipulation methods.[47] Traditional light-driven rotor systems typically require sophisticated laser beams or rotors with asymmetric geometry or nonuniform birefringence to get an optical torque.36,48,49 In comparison, our rotating robots can be sphere-symmetric and isotropic, and function with simple beams at low powers. Moreover, an on-demand control of rotation rate can be achieved by tuning the optical torque or the viscosity of the solution through the adjustment of the optical intensity or the concentration of PEG (Supplementary Figure S7).

As predicted by our model, the rolling (toward) mode (Figure 3c and Supplementary Movie S4) was achieved by aligning the laser beam about 1.3 μm away from the particle, i.e., $D_{P-L} \approx 1.3$ μm. The translation rate of the rolling particle was 0.81 μm/s at $I = 0.23\,\text{mW}/\mu\text{m}^2$. As D_{P-L} was further increased to 1.6–2.1 μm, the PS particle worked in the rolling (away) mode (Figure 3d and Supplementary Movie S5). The observed D_{P-L} is roughly 0.4 μm smaller than the theoretical value of 2 μm, which may result from the ignored thermal convection in the model. The particle rolled away from the laser beam at a small velocity of ~0.2 μm/s as I was increased to 1.2 mW/μm^2, because the temperature gradient and EM field around the particle were multiple times smaller compared to those of the previous working modes. The last working mode, the shooting mode, is shown in Figure 3e (also see Supplementary Movie S6). Briefly, one PS particle (left) is illuminated by the beam and functions as a hot spot generating repulsive forces that shoot out the other PS bead (right). Since F_{TE} is always larger than F_D in the current system as shown in Figure 2a, any negatively charged micro/nanoparticle, such as the second PS particle shown in Figure 3e, will experience a repulsive force. Distinct from direct manipulation, such as tweezing or pushing, the shooting mode shows the advantage of long-distance manipulation in a phototoxicity-free manner. The local temperatures of the particle center in different modes are shown in Supplementary Figure S8.

The general applicability of the multimodal manipulation platform has been validated by manipulating silicon (Si) micro/nanoparticles multimodally in control experiments. As shown in Supplementary Figure S9, the maximum temperature rise of a heated 1.5-μm Si particle[50] is ~7 K under the illumination of a 532 nm beam at $I = 0.064\,\text{mW}/\mu\text{m}^2$. Leveraging the optothermal forces generated from the self-generated temperature fields, we successfully realized tweezing, rotating, and rolling of a 1.5-μm Si microbead (Supplementary Movie S7). In theory, it is also possible to multimodally manipulate subwavelength targets (Supplementary Figure S10), while it could be challenging to achieve the adjustment of D_{P-L} in the subwavelength range for different manipulation modes. The control experiments demonstrate the versatility of the platform for the manipulation of objects with different sizes and materials.

On-Demand Control of Live Cells.

The capability to precisely manipulate single cells plays a critical role in fundamental studies in cellular biology. For instance, the controllable translation and rotation of cells can be utilized as single-cell assays to investigate cell–cell interactions and receptor–ligand binding for immunotherapy.[29,51,52] Indirect manipulations of cells using a microparticle trapped by optical tweezers have been developed to reduce the optical power requested for optical manipulation of cells.[53] However, the optical rotation of single cells is still extremely challenging. External fields or sophisticated microstructures manipulated by multibeam have been used to achieve single-cell rotation.[54-56]

To explore the potential applications of the multimodal manipulation platform in cellular biology, we investigate its capability for single-cell manipulation using a single beam. As a preliminary demonstration, we achieved on-demand translation and rotation of live yeast cells (*Saccharomyces cerevisiae*) by steering a 2.8-μm PS bead as a microbot. A

low-power beam ($I < 0.1\ \mathrm{mW}\ /\ \mu\mathrm{m}^2$) was used for all single-cell experiments to minimize thermal damage. As shown in Figure 4a, a PS microparticle was actuated remotely with a 532 nm laser to achieve the delivery of a yeast cell (also see Supplementary Movie S8). The cell was picked up, transported, and released at the target position using a low-power beam in 35 s. The cell delivery relies on the entropic attraction induced by the depletion of polymer molecules (i.e., PEG molecules).[57] Besides translational manipulation, we managed to control the rotational motions of yeast cells (Figure 4b). First, the PS particle was brought to be in contact with the yeast cell. Then, the beam was gradually moved from the particle center toward the cell ($D_{\mathrm{P-L}} = 1\ \mu\mathrm{m}$) to switch to the rotating mode. Next, the yeast cell started rotating along with the spinning particle due to the tangential rolling friction generated from the normal attraction between them (see Supplementary Movie S9). Moreover, a selective single-cell rotation of two yeast cells contacting each other was achieved by regulating the rotation direction of the PS particle. By gradually shifting the beam, we achieved the rotation of the left yeast cell followed by the rotation of the right yeast cell (see Figures 4c and 4d, and Supplementary Movie S10). It should be noted that only tweezing and rotating modes can be achieved herein because there are only one attractive force and one torque acting on the cells. Despite the high biocompatibility of PS particles, tiny particles that are made of biomolecules such as lipids, starch, and cellulose could be more biocompatible.[58] Among them, particles exhibiting proper light absorption can be ideal alternative substances for cell manipulation. For instance, plasmonic vesicles,[59] consisting of lipids and gold nanoparticles, are highly biocompatible and can convert light to heat for cell manipulation on this platform. We note that direct operation of living cells (without steering a microparticle) might be achieved by heating the liquid surrounding the target cells through multiphoton absorption induced by a pulsed laser beam (e.g., femtosecond laser).[60] However, the short-$D_{\mathrm{P-L}}$ manipulation modes, such as tweezing, could cause damage to cells due to the light absorption by the cells. With its versatile control of both translational and rotational motions for single cells, our multimodal micro/nanomanipulation platform could serve as an effective tool for single-cell studies.

Single-Particle Manipulation on Living Animal Embryos.

Besides cell manipulation, our platform stands out for remote particle manipulation on the biological surfaces of living small animals. *C. elegans* are 1 mm-long, transparent nematodes. They have been widely adopted as model organisms in biomedical-related research due to their short reproductive cycle, stereotyped development, optical transparency, and the genetics tools that are available. We, therefore, tested whether we could apply our technology to manipulate particles on living *C. elegans* embryos and larvae. As shown in Figure 5a, a 2.8-μm PS particle can be manipulated in contact with a *C. elegans* embryo (see Supplementary Movie S11). A target PS particle and a reference PS particle were first moved near the embryo. Then, the target particle was lifted with the radiation pressure by increasing I to 1.8 $\mathrm{mW}/\mu\mathrm{m}^2$ until the particle reached the top surface of the embryo as observed from the defocusing of the reference particle. Last, the PS particle was grasped by the trap well formed by the depletion force and moved arbitrarily on the embryo at $I = 0.11\ \mathrm{mW}\ /\ \mu\mathrm{m}^2$ to demonstrate the versatility of the platform. Continued development was observed for all embryos after manipulation, suggesting limited damage to embryos

(Supplementary Figure S11). We further demonstrate the manipulation of an 800 nm Si particle on a living L1 stage *C. elegans* larva (Figure 5b) to meet the requirements for studies of active animals. As shown in Supplementary Movie S12, despite the active movement of the animal, we successfully moved the Si nanoparticle back and forth on a living worm.

Our platform may serve as a promising tool for the studies of local thermodynamics in worms[61] or other biological samples by directing light-absorbing particles to the target positions and followed by optical heating. In contrast, it is challenging for conventional optical tweezers to achieve simultaneous manipulation and optical heating as the strong Brownian motion induced by the heat could shadow the optical trap well. As shown in Supplementary Figure S12 and Supplementary Movie S13, an 800 nm Si particle was steered to move around near the head of a *C. elegans* larva about to hatch for thermal stimulation. Interestingly, a potential thermal response of the larva was observed. The tail of the larva inside the embryo was found beating at a frequency of ~0.25 Hz during the process of *in vivo* manipulation. The beating frequency was around 0.08 Hz when the larva is illuminated by the incident light without heating a Si nanoparticle.

CONCLUSIONS

In summary, we have developed a multimodal optothermal manipulation platform that can operate on various surfaces, including the highly rough surfaces of small living animals. By regulating both the translational and rotational momenta of light-absorbing micro/nanoparticles, five different manipulation modes have been realized and can be switched on demand by simply controlling the laser-particle distance or optical power intensity. The versatile manipulation of micro/nanoparticles is driven by the synergy of thermal and optical forces. We have further developed a physical model to quantitatively understand the origin of forces and torques that dictate the different locomotion behaviors, shedding light on the rational design and optimization of the platform for targeted applications. The demonstrated manipulation of particles on living worms and embryos highlights the advanced applications of this platform in cellular biology.

METHODS

Optical Setup.

A laser beam at the wavelength of 660 nm (Laser Quantum, Opus 660) or 532 nm (Coherent, Genesis MX STM-1W) was expanded with a 5× beam expander (Thorlabs, GBE05-A) and introduced to a Nikon inverted microscope (Nikon, Ti-E) with a 100× oil objective (Nikon, CFI Plan Fluor 100XS Oil) for the manipulation experiments inside a microfluidic chamber of ~120 μm thickness. A complementary metal-oxide-semiconductor (CMOS) camera (Nikon, DS-Fi3) was used to obtain the optical images and videos. When necessary, a notch filter was put between the objective and the camera to block the incident laser beam. Fluorescence images were taken by using a xenon lamp (Sutter Instrument Lambda, LB-LS/30) with a green fluorescent protein (GFP) filter cube (457–487/502–538 nm).

Sample Preparation.

A 15 μL PEG/NaCl solution with particles, cells, or living organisms was added on a glass substrate with a spacer (Secure-Seal), and then an 18 × 18 mm^2 coverslip (Thermo Fisher Scientific) was placed on the top, creating a liquid film (thickness: 120 μm) between the coverslip and the glass substrate. The substrate with a thin layer of bovine serum albumin (BSA) to avoid stochastic adhesion was fabricated by immersing 22 × 22 mm^2 glass slides (Thermo Fisher Scientific) in a phosphate-buffered saline (PBS) solution with 1% BSA (Sigma-Aldrich, A8531) at room temperature for 24 h, followed by rinsing with DI water (Milli-Q) and drying under a nitrogen stream. A 4.5 wt % PEG 20000 powder (Sigma-Aldrich, 8.18897) and a 1% particle/cell solution were dissolved in a diluted NaCl solution to obtain the targeted PEG/NaCl solution. To disperse the particles uniformly, an ultrasonic bath (Branson, CPX5800H) was used. A suspension of 1 wt % 2.8 μm PS beads containing 12% iron dioxide (Thermo Fisher Scientific, 65306) was diluted with a 5 mM NaCl solution by 1000 times. The fluorescent labeling was conducted by mixing the NaCl solution containing the PS beads with a 1‰ 40 nm yellow-green fluorescent (505/515), biotin-labeled nanobeads suspension (Thermo Fisher Scientific, F8766). Then, the mixed solution was stored at 4 °C for 12 h, followed by centrifugation at 8,000 rpm for 5 min at room temperature. Yeast cells (Red Star) were washed three times and resuspended in DI water to obtain a cell density of ~5 × 10^5 cells/mL.

Worm Handling.

C. elegans (wild-type N2 strain) were fed with OP50 *E. coli* and maintained on a standard NGM growth medium at 20 °C. Embryos and larvae were examined before sex can be determined; however, most embryos and larvae were likely to be hermaphrodites, because the spontaneous occurrence of males without mating is rare. For imaging experiments, embryos were dissected in a drop of water and transferred to PEG/NaCl solution using a glass microneedle.

Numerical Simulations.

COMSOL Multiphysics (ver. 5.4a) was used in simulations based on FEM to calculate the optical forces, light-to-heat conversion, and temperature distributions. Specifically, modules of wave optics, heat transfer in solids, heat transfer in liquids, laminar flow, and multiphysics across these modules were used to simulate the physics of laser heating of light-absorbing particles. A particle was introduced on a substrate at varying positions with respect to the laser beam axis. The electromagnetic fields inside the particle, evaluated using the wave optics module, were used to calculate the electromagnetic heating of the particle. The heat transfer modules were used to obtain the temperature distribution around the particle. The temperatures on the substrate and the particle surface were exported as a discrete data set, based on which the depletion and thermoelectric forces were then computed in MATLAB (ver. 2020). Modeling details are summarized in Supplementary Note S1, including the modeling framework, governing equations, and boundary conditions.

Temperature Measurements.

Microscale temperature fields were measured through thermal imaging with quadriwave shearing interferometry (TIQSI).[62] A high-resolution wavefront sensor (SID4-HR, Phasics) was coupled with the inverted microscope with a ×100 oil objective. Thermal images were obtained by processing phase images using SIDFTHERMO software (Phasics).

Supplementary Material

Refer to Web version on PubMed Central for supplementary material.

ACKNOWLEDGMENTS

H.D., P.S.K., K.Y., and Y.Z. acknowledge the financial support of the National Institute of General Medical Sciences of the National Institutes of Health (R01GM146962) and the National Science Foundation (NSF-ECCS-2001650). Y.C. acknowledges the financial support of a UT Austin Provost's Graduate Education Fellowship. D.J.D. is a CPRIT scholar supported by the Cancer Prevention and Research Institute of Texas (RR170054). D.J.D. additionally acknowledges the financial support of the NIH-NIGMS (R01 GM138443 and R21 GM144817). The authors are grateful to Prof. Brian A. Korgel and Dr. Taizhi Jiang for providing Si micro/nanoparticles. We thank the Texas Advanced Computing Centre (TACC) at UT Austin for providing HPC resources that contributed to the research results reported in this paper. URL: http://www.tacc.utexas.edu.

REFERENCES

(1). Ashkin A; Dziedzic JM; Bjorkholm JE; Chu S Observation of a Single-Beam Gradient Force Optical Trap for Dielectric Particles. Opt. Lett 1986, 11, 288–290. [PubMed: 19730608]

(2). Killian JL; Ye F; Wang MD Optical Tweezers: A Force to Be Reckoned With. Cell 2018, 175, 1445–1448. [PubMed: 30500527]

(3). Singh VA; Sitti M Targeted Drug Delivery and Imaging Using Mobile Milli/Microrobots: A Promising Future Towards Theranostic Pharmaceutical Design. Curr. Pharm. Des 2016, 22, 1418–1428. [PubMed: 26654436]

(4). Blazquez-Castro A Optical Tweezers: Phototoxicity and Thermal Stress in Cells and Biomolecules. Micromachines (Basel) 2019, 10, 507. [PubMed: 31370251]

(5). Chen Z; Li J; Zheng Y Heat-Mediated Optical Manipulation. Chem. Rev 2022, 122, 3122–3179. [PubMed: 34797041]

(6). Franzl M; Thalheim T; Adler J; Huster D; Posseckardt J; Mertig M; Cichos F Thermophoretic Trap for Single Amyloid Fibril and Protein Aggregation Studies. Nat. Methods 2019, 16, 611–614. [PubMed: 31235884]

(7). Li J; Chen Z; Liu Y; Kollipara PS; Feng Y; Zhang Z; Zheng Y Opto-Refrigerative Tweezers. Sci. Adv 2021, 7, No. eabh1101. [PubMed: 34172454]

(8). Lin L; Wang M; Peng X; Lissek EN; Mao Z; Scarabelli L; Adkins E; Coskun S; Unalan HE; Korgel BA; Liz-Marzan LM; Florin EL; Zheng Y Opto-Thermoelectric Nanotweezers. Nat. Photonics 2018, 12, 195–201. [PubMed: 29785202]

(9). Wang X; Yuan Y; Xie X; Zhang Y; Min C; Yuan X Graphene-Based Opto-Thermoelectric Tweezers. Adv. Mater 2022, 34, No. e2107691. [PubMed: 34897844]

(10). Ndukaife JC; Kildishev AV; Nnanna AG; Shalaev VM; Wereley ST; Boltasseva A Long-Range and Rapid Transport of Individual Nano-Objects by a Hybrid Electrothermoplasmonic Nanotweezer. Nat. Nanotechnol 2016, 11, 53–9. [PubMed: 26524398]

(11). Hong C; Yang S; Ndukaife JC Stand-Off Trapping and Manipulation of Sub-10 Nm Objects and Biomolecules Using Opto-Thermo-Electrohydrodynamic Tweezers. Nat. Nanotechnol 2020, 15, 908–913. [PubMed: 32868919]

(12). Jiang HR; Wada H; Yoshinaga N; Sano M Manipulation of Colloids by a Nonequilibrium Depletion Force in a Temperature Gradient. Phys. Rev. Lett 2009, 102, 208301. [PubMed: 19519079]

(13). Braun D; Libchaber A Trapping of DNA by Thermophoretic Depletion and Convection. Phys. Rev. Lett 2002, 89, 188103. [PubMed: 12398641]

(14). Liu Y; Lin L; Bangalore Rajeeva B; Jarrett JW; Li X; Peng X; Kollipara P; Yao K; Akinwande D; Dunn AK; Zheng Y Nanoradiator-Mediated Deterministic Opto-Thermoelectric Manipulation. ACS Nano 2018, 12, 10383–10392. [PubMed: 30226980]

(15). Alam MS; Zhan Q; Zhao C Additive Opto-Thermomechanical Nanoprinting and Nanorepairing under Ambient Conditions. Nano Lett. 2020, 20, 5057–5064. [PubMed: 32502352]

(16). Zhao C; Shah PJ; Bissell LJ Laser Additive Nano-Manufacturing under Ambient Conditions. Nanoscale 2019, 11, 16187–16199. [PubMed: 31461093]

(17). Khadka U; Holubec V; Yang H; Cichos F Active Particles Bound by Information Flows. Nat. Commun 2018, 9, 3864. [PubMed: 30242284]

(18). Li J; Liu Y; Lin L; Wang M; Jiang T; Guo J; Ding H; Kollipara PS; Inoue Y; Fan D; Korgel BA; Zheng Y Optical Nanomanipulation on Solid Substrates Via Optothermally-Gated Photon Nudging. Nat. Commun 2019, 10, 5672. [PubMed: 31831746]

(19). Qian B; Montiel D; Bregulla A; Cichos F; Yang H Harnessing Thermal Fluctuations for Purposeful Activities: The Manipulation of Single Micro-Swimmers by Adaptive Photon Nudging. Chem. Sci 2013, 4, 1420–1429.

(20). Lin L; Kollipara PS; Kotnala A; Jiang T; Liu Y; Peng X; Korgel BA; Zheng Y Opto-Thermoelectric Pulling of Light-Absorbing Particles. Light Sci. Appl 2020, 9, 34. [PubMed: 32194948]

(21). Sharma V; Tiwari S; Paul D; Sahu R; Chikkadi V; Kumar GVP Optothermal Pulling, Trapping, and Assembly of Colloids Using Nanowire Plasmons. Soft Matter 2021, 17, 10903–10909. [PubMed: 34807220]

(22). Ding H; Chen Z; Ponce C; Zheng Y Optothermal Rotation of Micro-/Nano-Objects. Chem. Commun. (Camb.) 2023, 59, 2208–2221. [PubMed: 36723196]

(23). Ding H; Kollipara PS; Kim Y; Kotnala A; Li J; Chen Z; Zheng Y Universal Optothermal Micro/Nanoscale Rotors. Sci. Adv 2022, 8, No. eabn8498. [PubMed: 35704582]

(24). Nagelberg S; Totz JF; Mittasch M; Sresht V; Zeininger L; Swager TM; Kreysing M; Kolle M Actuation of Janus Emulsion Droplets Via Optothermally Induced Marangoni Forces. Phys. Rev. Lett 2021, 127, 144503. [PubMed: 34652186]

(25). Kim H; Sundaram S; Kang JH; Tanjeem N; Emrick T; Hayward RC Coupled Oscillation and Spinning of Photothermal Particles in Marangoni Optical Traps. Proc. Natl. Acad. Sci. U. S. A 2021, 118, No. e2024581118. [PubMed: 33903243]

(26). Lin L; Peng X; Wei X; Mao Z; Xie C; Zheng Y Thermophoretic Tweezers for Low-Power and Versatile Manipulation of Biological Cells. ACS Nano 2017, 11, 3147–3154. [PubMed: 28230355]

(27). Littman ML Reinforcement Learning Improves Behaviour from Evaluative Feedback. Nature 2015, 521, 445–51. [PubMed: 26017443]

(28). Ding H; Chen Z; Kollipara PS; Liu Y; Kim Y; Huang S; Zheng Y Programmable Multimodal Optothermal Manipulation of Synthetic Particles and Biological Cells. ACS Nano 2022, 16, 10878–10889. [PubMed: 35816157]

(29). Liu Y; Ding H; Li J; Lou X; Yang M; Zheng Y Light-Driven Single-Cell Rotational Adhesion Frequency Assay. eLight 2022, 2, 13. [PubMed: 35965781]

(30). Duhr S; Braun D Why Molecules Move Along a Temperature Gradient. Proc. Natl. Acad. Sci. U. S. A 2006, 103, 19678–82. [PubMed: 17164337]

(31). Maeda YT; Tlusty T; Libchaber A Effects of Long DNA Folding and Small Rna Stem-Loop in Thermophoresis. Proc. Natl. Acad. Sci. U. S. A 2012, 109, 17972–7. [PubMed: 23071341]

(32). Ding H; Kollipara PS; Lin L; Zheng Y Atomistic Modeling and Rational Design of Optothermal Tweezers for Targeted Applications. Nano Res. 2021, 14, 295–303. [PubMed: 35475031]

(33). Chen Z; Kollipara PS; Ding H; Pughazhendi A; Zheng Y Liquid Optothermoelectrics: Fundamentals and Applications. Langmuir 2021, 37, 1315–1336. [PubMed: 33410698]

(34). Reichl M; Herzog M; Gotz A; Braun D Why Charged Molecules Move across a Temperature Gradient: The Role of Electric Fields. Phys. Rev. Lett 2014, 112, 198101. [PubMed: 24877967]

(35). Ashkin A; Dziedzic JM; Yamane T Optical Trapping and Manipulation of Single Cells Using Infrared Laser Beams. Nature 1987, 330, 769–71. [PubMed: 3320757]

(36). Shao L; Käll M Light-Driven Rotation of Plasmonic Nanomotors. Adv. Funct. Mater 2018, 28, 1706272.

(37). Jackson JD Maxwell Equations, Macroscopic Electromagnetism, Conservation Laws. In Classical Electrodynamics, 3rd ed.; John Wiley & Sons: New York, 1999; p 261.

(38). Du J; Yuen C-H; Li X; Ding K; Du G; Lin Z; Chan CT; Ng J Tailoring Optical Gradient Force and Optical Scattering and Absorption Force. Sci. Rep 2017, 7, 18042. [PubMed: 29273791]

(39). Bradac C Nanoscale Optical Trapping: A Review. Adv. Opt. Mater 2018, 6, 1800005.

(40). Kim Y; Ding H; Zheng Y Enhancing Surface Capture and Sensing of Proteins with Low-Power Optothermal Bubbles in a Biphasic Liquid. Nano Lett. 2020, 20, 7020–7027. [PubMed: 32667815]

(41). Bregulla AP; Würger A; Gunther K; Mertig M; Cichos F Thermo-Osmotic Flow in Thin Films. Phys. Rev. Lett 2016, 116, 188303. [PubMed: 27203347]

(42). Gargiulo J; Brick T; Violi IL; Herrera FC; Shibanuma T; Albella P; Requejo FG; Cortes E; Maier SA; Stefani FD Understanding and Reducing Photothermal Forces for the Fabrication of Au Nanoparticle Dimers by Optical Printing. Nano Lett. 2017, 17, 5747–5755. [PubMed: 28806511]

(43). Heidari M; Bregulla A; Muinos Landin S; Cichos F; von Klitzing R Self-Propulsion of Janus Particles near a Brush-Functionalized Substrate. Langmuir 2020, 36, 7775–7780. [PubMed: 32544339]

(44). Majee A; Wurger A Thermocharge of a Hot Spot in an Electrolyte Solution. Soft Matter 2013, 9, 2145–2153.

(45). Putnam SA; Cahill DG Transport of Nanoscale Latex Spheres in a Temperature Gradient. Langmuir 2005, 21, 5317–23. [PubMed: 15924455]

(46). Wurger A Transport in Charged Colloids Driven by Thermoelectricity. Phys. Rev. Lett 2008, 101, 108302. [PubMed: 18851262]

(47). Huang L; Zhao P; Liang F; Wang W Single-Cell 3d Electro-Rotation. Methods Cell Biol. 2018, 148, 97–116. [PubMed: 30473076]

(48). Sipova-Jungova H; Andren D; Jones S; Kall M Nanoscale Inorganic Motors Driven by Light: Principles, Realizations, and Opportunities. Chem. Rev 2020, 120, 269–287. [PubMed: 31869216]

(49). Shao L; Yang ZJ; Andren D; Johansson P; Kall M Gold Nanorod Rotary Motors Driven by Resonant Light Scattering. ACS Nano 2015, 9, 12542–51. [PubMed: 26564095]

(50). Harris JT; Hueso JL; Korgel BA Hydrogenated Amorphous Silicon (a-Si:H) Colloids. Chem. Mater 2010, 22, 6378–6383.

(51). Huang J; Zarnitsyna VI; Liu B; Edwards LJ; Jiang N; Evavold BD; Zhu C The Kinetics of Two-Dimensional Tcr and Pmhc Interactions Determine T-Cell Responsiveness. Nature 2010, 464, 932–6. [PubMed: 20357766]

(52). Zhang Z; Ahmed D Light-Driven High-Precision Cell Adhesion Kinetics. Light Sci. Appl 2022, 11, 266. [PubMed: 36100594]

(53). Banerjee AG; Chowdhury S; Losert W; Gupta SK Survey on Indirect Optical Manipulation of Cells, Nucleic Acids, and Motor Proteins. J. Biomed. Opt 2011, 16, 051302. [PubMed: 21639562]

(54). Vizsnyiczai G; Buzas A; Lakshmanrao Aekbote B; Fekete T; Grexa I; Ormos P; Kelemen L Multiview Microscopy of Single Cells through Microstructure-Based Indirect Optical Manipulation. Biomed. Opt. Express 2020, 11, 945–962. [PubMed: 32133231]

(55). Kolb T; Albert S; Haug M; Whyte G Optofluidic Rotation of Living Cells for Single-Cell Tomography. J. Biophotonics 2015, 8, 239–46. [PubMed: 24733809]

(56). Ahmed D; Ozcelik A; Bojanala N; Nama N; Upadhyay A; Chen Y; Hanna-Rose W; Huang TJ Rotational Manipulation of Single Cells and Organisms Using Acoustic Waves. Nat. Commun 2016, 7, 11085. [PubMed: 27004764]

(57). Feng L; Laderman B; Sacanna S; Chaikin P Re-Entrant Solidification in Polymer-Colloid Mixtures as a Consequence of Competing Entropic and Enthalpic Attractions. Nat. Mater 2015, 14, 61–5. [PubMed: 25326826]

(58). Ranjha M; Shafique B; Rehman A; Mehmood A; Ali A; Zahra SM; Roobab U; Singh A; Ibrahim SA; Siddiqui SA Biocompatible Nanomaterials in Food Science, Technology, and Nutrient Drug Delivery: Recent Developments and Applications. Front. Nutr 2022, 8, 778155. [PubMed: 35127783]

(59). Xiong H; Li X; Kang P; Perish J; Neuhaus F; Ploski JE; Kroener S; Ogunyankin MO; Shin JE; Zasadzinski JA; Wang H; Slesinger PA; Zumbuehl A; Qin Z Near-Infrared Light Triggered-Release in Deep Brain Regions Using Ultra-Photosensitive Nanovesicles. Angew. Chem., Int. Ed. Engl 2020, 59, 8608–8615. [PubMed: 32124529]

(60). Longtin JP; Tien C-L Efficient Laser Heating of Transparent Liquids Using Multiphoton Absorption. Int. J. Heat Mass Transfer 1997, 40, 951–959.

(61). Fritsch AW; Diaz-Delgadillo AF; Adame-Arana O; Hoege C; Mittasch M; Kreysing M; Leaver M; Hyman AA; Julicher F; Weber CA Local Thermodynamics Govern Formation and Dissolution of Caenorhabditis Elegans P Granule Condensates. Proc. Natl. Acad. Sci. U. S. A 2021, 118, No. e2102772118. [PubMed: 34507991]

(62). Baffou G; Bon P; Savatier J; Polleux J; Zhu M; Merlin M; Rigneault H; Monneret S Thermal Imaging of Nanostructures by Quantitative Optical Phase Analysis. ACS Nano 2012, 6, 2452–8. [PubMed: 22305011]

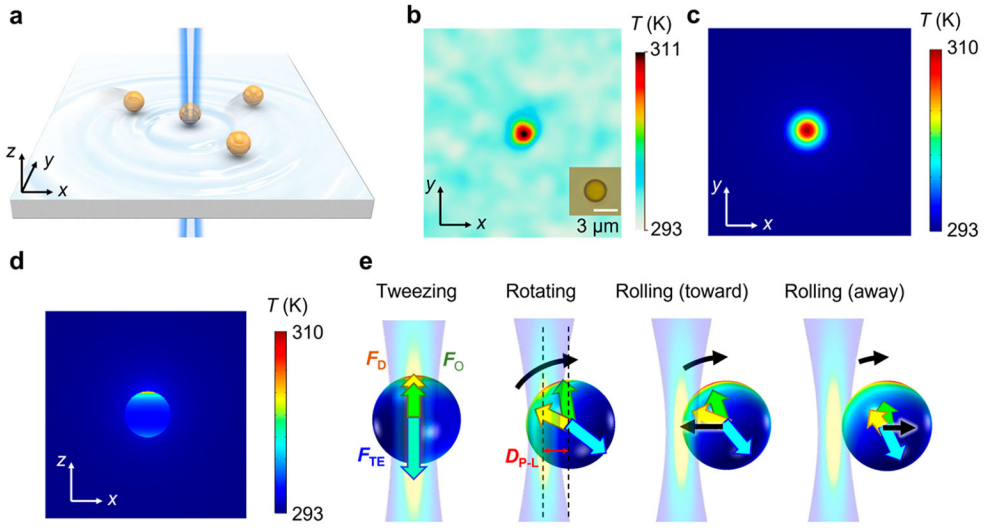

Figure 1.

Working principle of multimodal optical manipulation with self-powered temperature fields. (a) A simplified schematic illustrating the experimental setup and operation for the multimodal manipulation of micro/nanoparticles in a liquid on a glass substrate with self-sustained temperature fields. (b) The measured temperature distribution on the XY plane when a 2.8-μm PS particle was heated by a 532 nm laser beam (optical power intensity: 0.23 mW/μm^2). Inset: the optical image of the PS particle immersed in the solution. Scale bar: 3 μm. (c,d) Simulated temperature distributions on the XY plane and the XZ plane. (e) Tweezing, rotating, rolling (toward), and rolling (away) of the particle are achieved in order by gradually increasing D_{P-L} under the effect of F_D (yellow arrow), F_{TE} (blue arrow), and F_O (green arrow). The temperature distribution on the particle surface changes with D_{P-L}, which directly alters the magnitude and direction of the thermal forces (F_D and F_{TE}). Meanwhile, the local electromagnetic (EM) field changes with D_{P-L}, resulting in distance-dependent F_O and the optical torque acting on the particle. The spot size of the beam for the tweezing mode is 2 μm, while that for other modes is 0.7 μm.

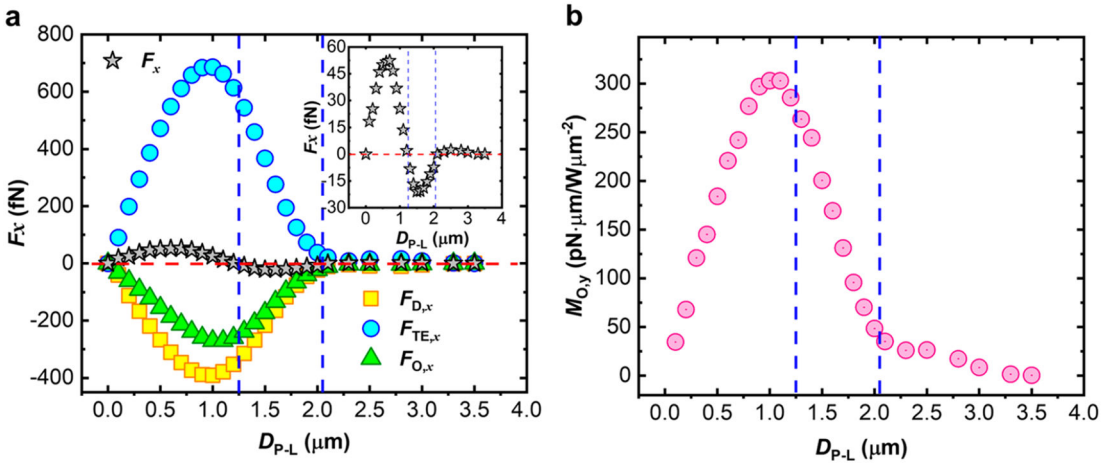

Figure 2.

Force and torque analysis of multimodal manipulation. (a) Simulated forces acting on a 2.8-μm PS particle along the x-axis as a function of the distance between the particle and the laser beam, D_{P-L}. F_x, $F_{D,x}$, $F_{TE,x}$, and $F_{O,x}$ are the net force (gray stars), depletion force (yellow squares), TE force (blue circles), and optical force (green triangles), respectively. Inset: a zoom-in figure for F_x. (b) Simulated optical torque relative to the y-axis at the particle center, $M_{O,y}$, as a function of D_{P-L}. The blue dashed line on the left marks the critical D_{P-L} where the rotating mode is achieved. The blue dashed line on the left marks the boundary between the rolling (toward) mode and the rolling (away) mode. The full-dimensional motion of the particle can be predicted from these two figures.

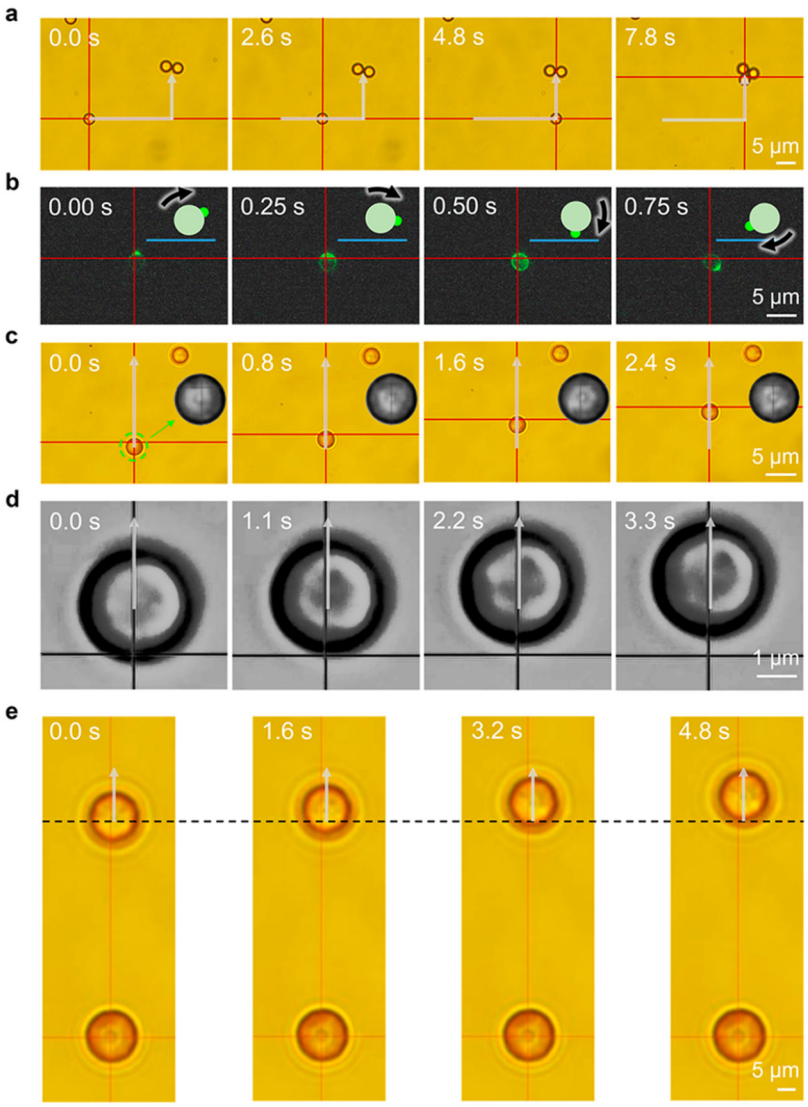

Figure 3.

Experimental demonstration of multimodal manipulation of microparticles. (a) Successive optical images of a trapped 2.8-μm PS particle being transported along a designed path denoted by the gray lines. The red cross marks the position of the incident light. (b) Successive fluorescence images of the rotating PS microparticle as the incident beam is positioned 1.1 μm away from the particle center. The green bright spot represents the attached 40 nm fluorescent beads on the surface of the PS microparticle. (c) Successive optical images showing the particle rolling toward the reference PS microparticle on the right top corner under the illumination of the beam 1.3 μm away. To show the orientation difference of the rolling particle, the close-up of the particle (the gray particle pointed by the green arrow) was postprocessed (decreasing saturation by 100% and increasing contrast by 100%) and put on the right. (d) Successive fluorescence images of the rolling (away) mode. D_{P-L} increases from 1.6 to 2.1 μm during the rolling process. The saturation and contrast of the images were decreased by 100% and increased by 100%, respectively. (e) Successive

fluorescence images showing the shooting mode. *I*: (a) 0.064 mW/μm^2, (b,c) 0.23 mW/μm^2, (d) 1.2 mW/μm^2, (e) 0.69 mW/μm^2. Scale bars: (a–c,e) 5 μm; (d) 1 μm.

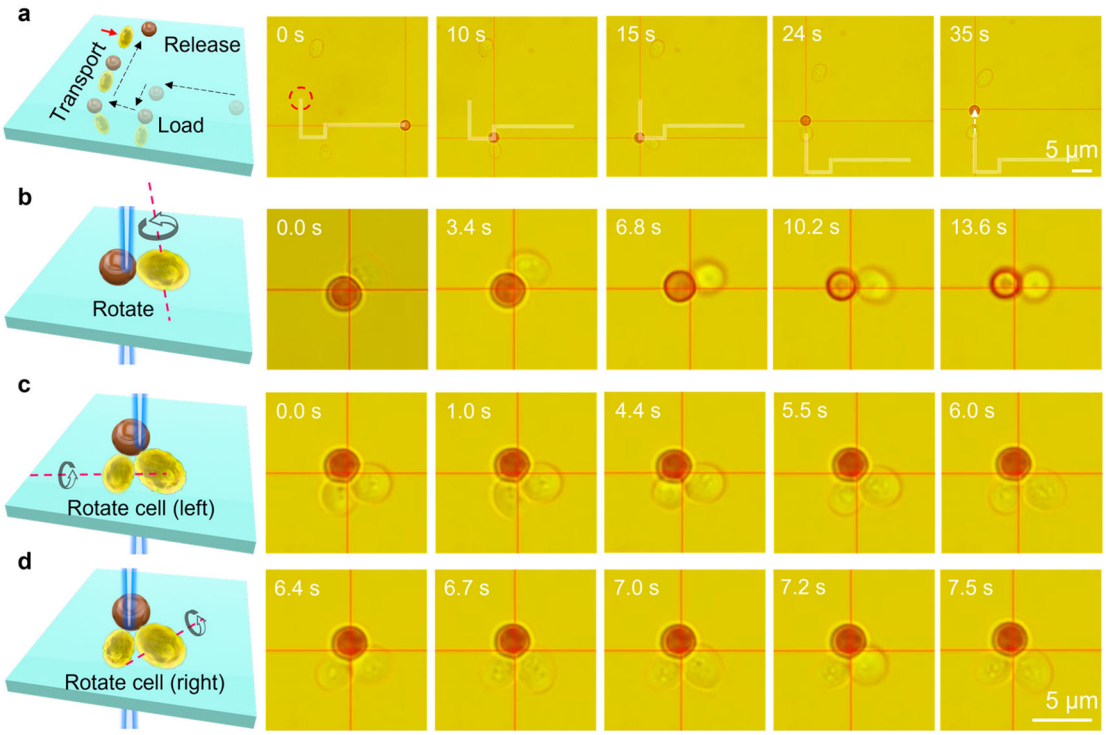

Figure 4.

Single-cell manipulation with a PS microbead. (a) Schematic (left) and successive images showing the delivery of a yeast cell using the tweezing mode. The red arrow and red circle in the schematic and the optical image mark the target position. The gray dashed lines and the white arrow in the optical images denote the designed path and release process, respectively. The red cross marks the position of the incident beam. (b) Rotation of a yeast cell by gradually increasing D_{P-L} to ~1 μm. (c,d) Selective rotation of two yeast cells in contact by repositioning the laser beam to tailor the rotation direction of the PS particle. I: 0.11 mW/μm^2. Scale bars: 5 μm.

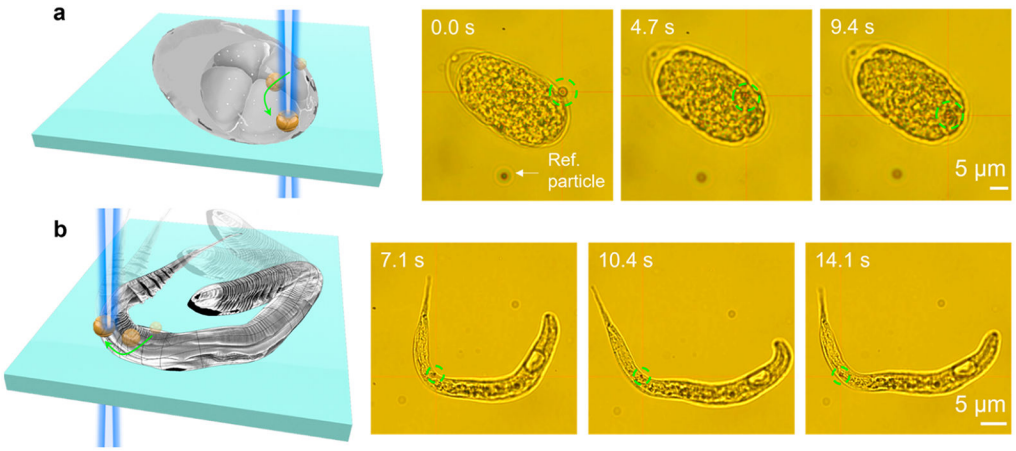

Figure 5.

Single-particle manipulation on living *C. elegans* and their embryos. (a) Schematic and time-resolved optical images demonstrating light-driven navigation of a 2.8-μm PS microbead on a *C. elegans* embryo. Another 2.8-μm PS particle on the glass substrate serves as a reference to show the changes in focal planes. (b) Schematic and time-solved optical images of an 800 nm Si particle moving on the surface of a living L1 stage *C. elegans* larva. I: 0.11 mW/μm^2. Scale bars: 5 μm.